Development of structural response diagram approach to evaluation of thermal stress caused by thermal striping

February, 1999

Oarai Engineering Center
Japan Nuclear Cycle Develoment Institute

Ⓐ

JNC TN9400 99-019
1 9 9 9 年 2 月

サーマルストライピングによる熱応力評価のための構造応答線図法の開発

(研究報告)

笠原 直人[1]、アピサラ ヤクンパイ[2] 、高正 英樹[3]

要 旨

原子力プラントの中で温度が異なる冷却材が合流する領域では、流体混合による不規則な温度ゆらぎが生じるため、熱応力による構造材の疲労破損に注意する必要がある。この現象はサーマルストライピングと称され、熱流体と構造が複雑に関連し合う現象であることから、従来はモックアップ実験による評価が行われており、簡便で合理的な設計評価法が必要とされていた。

これに対し、温度ゆらぎの振幅は流体から構造材への伝達過程において、乱流混合、分子拡散、非定常熱伝達、および熱伝導による温度除荷の各要因によって減衰し、その特性は周波数依存であることが解明されてきている。筆者らは、このうち非定常熱伝達と温度除荷の効果に着目し、両者による温度振幅の減衰効果を温度ゆらぎ周波数の関数として定量的に記述した構造応答線図を開発した。さらに本線図を設計へ応用するため、無次元数を導入することによって線図の一般化表示を行った。無次元化された構造応答線図の妥当性は、有限要素解析の結果との比較により検証した。本線図を利用することによって、流体温度ゆらぎ振幅から非定常熱伝達と温度除荷による減衰効果を考慮した熱応力の振幅を簡易に評価することが可能となる。

1) 大洗工学センター システム技術開発部 構造材料技術開発グループ
2) 大洗工学センター システム技術開発部 構造材料技術開発グループ (現 タイ原子力庁)
3) 常陽産業株式会社

Development of structural response diagram approach to evaluation of thermal stress caused by thermal striping

Naoto Kasahara[1], Apisara Yacumpai[2] ,and Hideki Takasho[3]

Abstract

At incomplete mixing area of high temperature and low temperature fluids near the surface of structures, temperature fluctuation of fluid gives thermal fatigue damage to wall structures. This thermohydraulic and thermomechanical coupled phenomenon is called thermal striping, which has so complex mechanism and sometimes causes crack initiation on the structural surfaces that rational evaluation methods are required for screening rules in design codes.

In this study, frequency response characteristics of structures and its mechanism were investigated by both numerical and theoretical methods. Based on above investigation, a structural response diagram was derived, which can predict stress amplitude of structures from temperature amplitude and frequency of fluids. Furthermore, this diagram was generalized to be the Non-dimensional structural response diagram by introducing non-dimensional parameters such as Biot number, non-dimensional frequency, and non-dimensional stress.

The use of the Non-dimensional structural response diagram appears to evaluate thermal stress caused by thermal striping, rapidly without structural analysis, and rationally with considering attenuation by non-stationary heat transfer and thermal unloading. This diagram can also give such useful information as sensitive frequency range to adjust coupled thermohydraulic and thermomechanical analysis models taking account of four kinds of attenuation factors: turbulent mixing, molecular diffusion, non-stationary heat transfer, and thermal unloading.

---

1) Structure and Material Research Group, System Engineering Division, OEC, JNC

2) Structure and Material Research Group, System Engineering Division, OEC, JNC
(Presently at OAEP, Thailand)

3) Joyo Industries Ltd.

Contents

List of Tables

List of Figures

1. Introduction

At incomplete mixing area of high temperature and low temperature fluids near the surface of structures, temperature fluctuation of fluid gives thermal fatigue damage to wall structures. This thermohydraulic and thermomechanical coupled phenomenon is called thermal striping, which has so complex mechanism and sometimes causes crack initiation on the structural surfaces that sodium mock-up tests are usually required to confirm structural integrity of components.

Recent investigation on thermal striping has revealed that amplitude of temperature fluctuation was attenuated during a series of heat transfer process from fluids to structures by ①turbulent mixing, ② molecular diffusion, ③non-stationary heat transfer, and ④thermal unloading as in Fig.1[1]. When taking these attenuation factors into consideration, rational evaluation against thermal striping will be realized[2].

However, the attenuation process is a thermal coupling problem between fluids and structures and has a sensitive characteristics to frequencies of temperature fluctuations. Therefore, time history analyses using coupled thermohydraulic and thermomechanical models are generally required to consider above factors.

Realizing time consuming coupled analysis methods are needed to be rationalized for adoption to screening rules in design codes, the authors commenced a development of new approaches, and recently the first results have been obtained.

Attention was given to the frequency response characteristics of structures caused from ③non-stationary heat transfer and ④thermal unloading as in Fig.1. Frequency response characteristics of structures will be investigated by F.E. calculation and by 1-D theory. Considering mechanism of structural response with attenuation factors ③and④, the Non-dimensional structural response diagram (NSRD) will be derived.

The use of the NSRD appears to evaluate thermal stress caused by thermal striping, rapidly without structural analysis, and rationally with considering attenuation from ③non-stationary heat transfer and ④thermal unloading. Another advantage of this approach is feedback from structural characteristics to thermal hydraulic analysis (Fig.2). For detailed evaluation taking above four kinds of attenuation factors into account, coupled thermohydraulic and thermomechanical models are required. To adjust those analysis models, NSRD can give such useful information as sensitive frequency range, which should be evaluated.

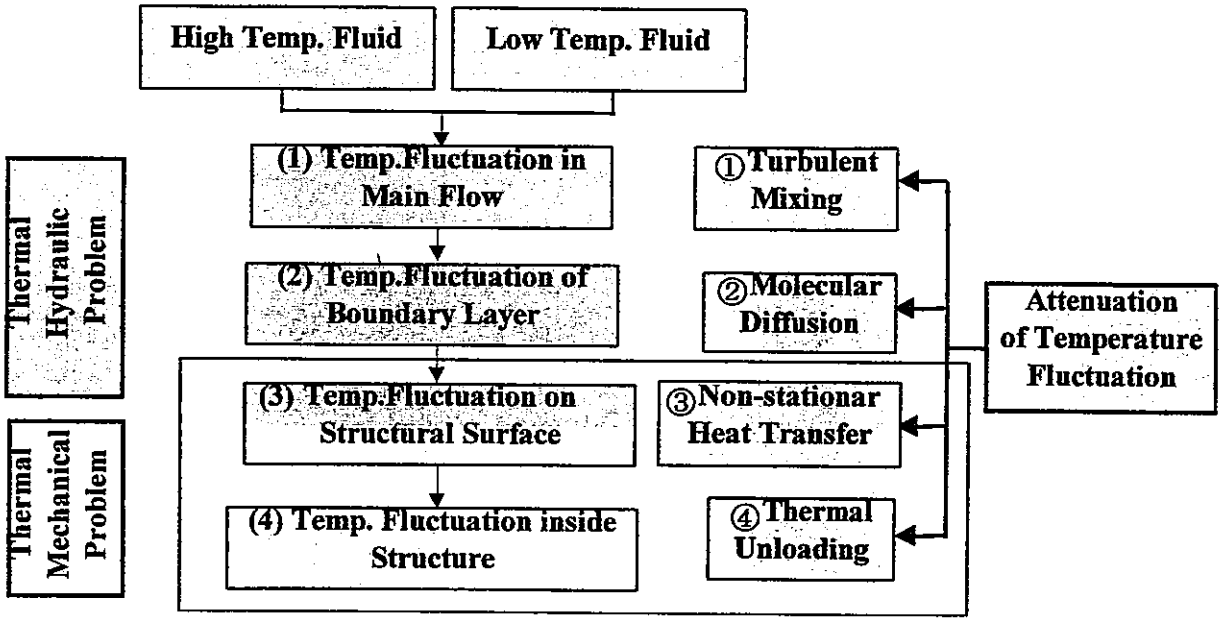

Fig.1 Attenuation factors of temperature fluctuation amplitude during a series of heat transfer process from fluid to structures

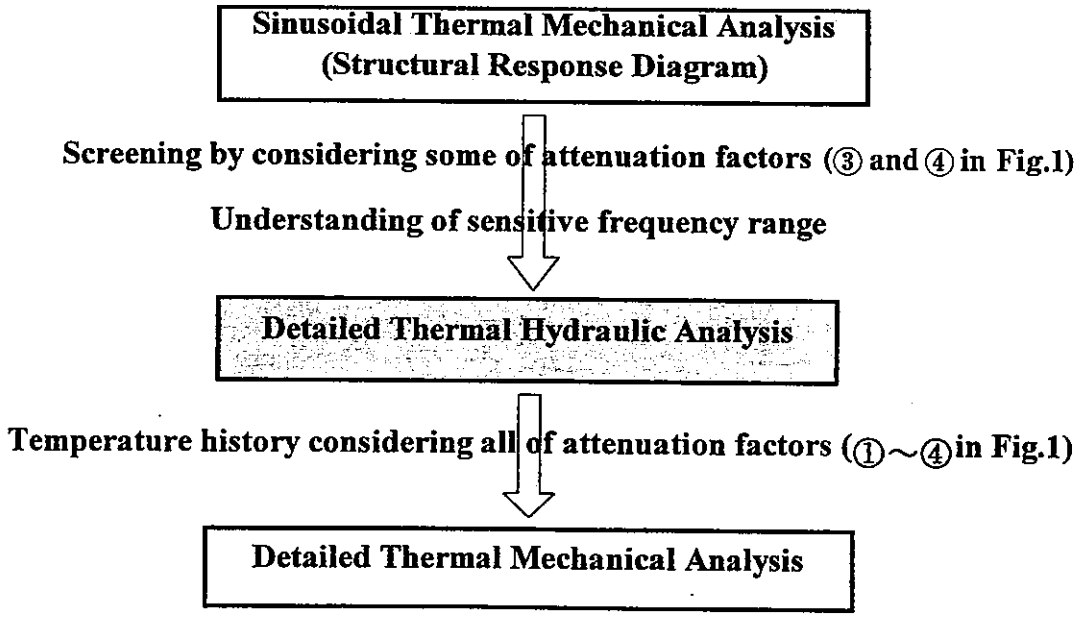

Fig.2 Concept of Structural Response Diagram Approach

2. Frequency response characteristics of a pipe wall

2.1 Finite element analysis conditions

In order to grasp sensitivity of structural responses to frequency of fluid temperature fluctuations, the pipe wall of Phenix secondary circuit[1] due to sinusoidal fluid temperature fluctuation with various frequencies was analyzed by FINAS code[3], which is a computer program based on the finite element method. Geometrical configuration, and thermal boundary condition are as shown in Fig.3, where wall thickness L is 7 mm, inner diameter is 494mm, and material is Type 304 stainless steel. The inner surface of the pipe is due to sinusoidal temperature fluctuation of fluid with constant amplitude ΔT_f as 90K (maximum temperature is 430 °C and minimum temperature is 340 °C) and the outer surface is kept insulated. This study assumed constant heat-transfer coefficient h, value of which was evaluated as 14500kcal/m^2*h*℃ from turbulent heat convection equation for liquid metal.

Frequencies of sinusoidal temperature fluctuation of fluid were varied as 0.01 Hz, 0.03 Hz, 0.07 Hz, 0.0846 Hz, 0.1 Hz, 1.0 Hz and 10 Hz.

Temperature distribution of structure $T_s(x,t)$ was calculated by solving the equation of transient heat conduction with a finite element model consists of the isoparametric 8-node quadrilateral axisymmetric heat conduction element HQAX8 and the isoparametric 3-node heat-transfer element FCAX3 of FINAS code. Where x is depth from the surface, and t is time. From calculated temperature distributions, induced thermal stresses in the structure were solved by thermal elastic analysis with a finite element model consists of the isoparametric 8-node quadrilateral axisymmetric element QAX8 of the same code.

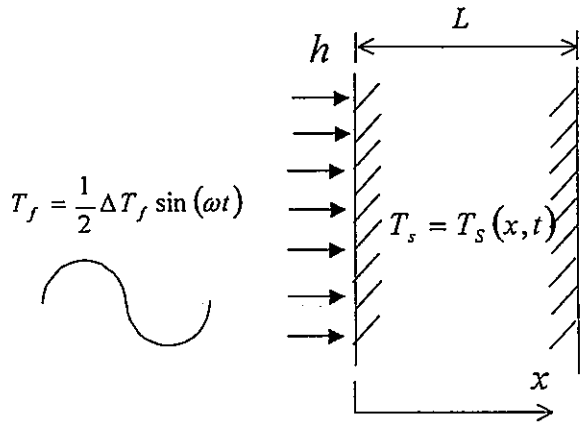

Fig.3 A pipe wall model due to sinusoidal temperature fluctuation

2.2 Heat conduction and thermal elastic analysis results

Heat conduction analysis results were summarized as in Fig. 4a- Fig.4g, which show the temperature histories at inner and outer surfaces under various frequencies of sinusoidal temperature fluctuation.

What is evident from these figures is that temperature amplitude decreases monotonously according to increase of frequency of fluctuation on both surfaces, among which the outer surface decreases rapidly than the inner surface. Its tendency is clear from Table 1, which shows temperature amplitude on the both surfaces. From different characteristics of both surfaces, temperature difference between the both surfaces distributes as in Fig.5.

The results of thermal elastic analysis were as in Fig. 6a- Fig.6g, which show stress histories at the inner and outer surfaces under various frequency of sinusoidal temperature fluctuation. The noteworthy point from above figures is that stress amplitude varies according to frequency and becomes the maximum at the particular frequency 0.0846Hz as in Table 2, even though amplitude of temperature fluctuation was constant. Fig.7 shows this effect clearly and allows the frequency response characteristics to be read quickly. Let us name a diagram in Fig.7 as a Structural Response Diagram(SRD).

The maximum stress can be read from Fig.7 as 243MPa at frequency of 0.0846Hz and it means that stress amplitude is always less than 243Mpa even though any kinds of random wave. Conventional thermal striping evaluation methods have adopted the next thermal elastic equation to calculate thermal stress range $\Delta\sigma$ from temperature amplitude ΔT[4].

$$\Delta\sigma = \frac{E\alpha}{1-\nu}\Delta T, \tag{1}$$

where E is Young's modulus, α is thermal expansion ratio, and ν is Poisson's ratio.

When substituting 90K to ΔT of Eq.(1), thermal stress range $\Delta\sigma$ is evaluated as 353MPa.
From this fact, SRD appears to evaluate thermal stress rationally than Eq.(1).

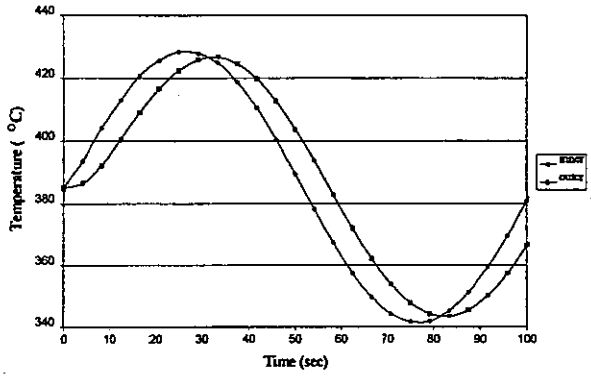

Fig.4a Temperature histories on the surfaces (0.01Hz)

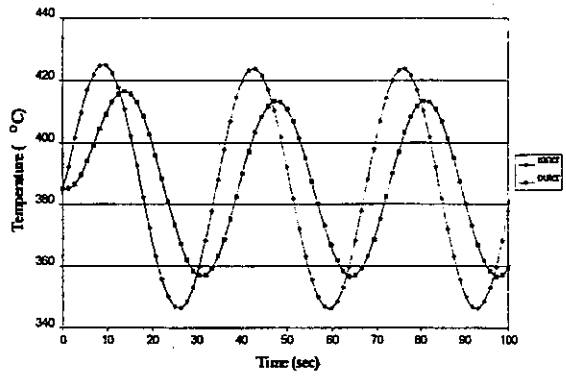

Fig.4b Temperature histories on the surfaces (0.03Hz)

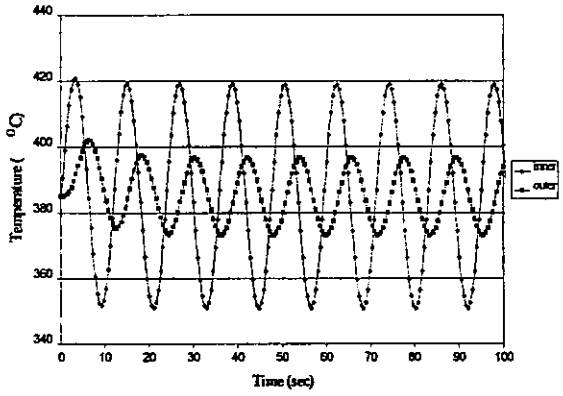

Fig.4c Temperature histories on the surfaces (0.07Hz)

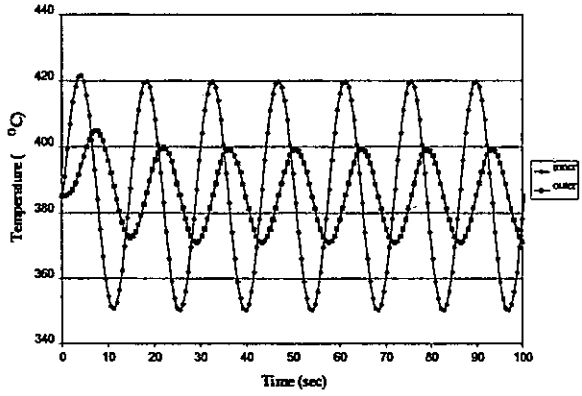

Fig.4d Temperature histories on the surfaces (0.0846Hz)

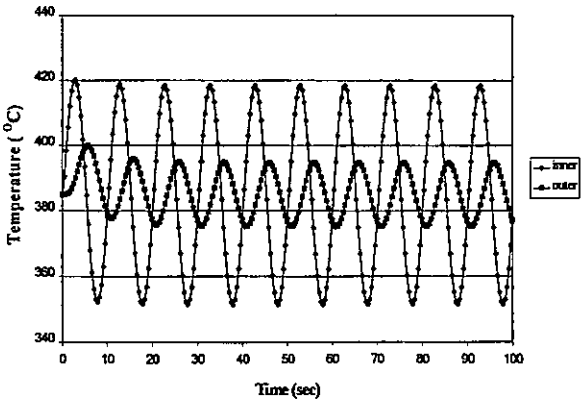

Fig.4e Temperature histories on the surfaces (0.1Hz)

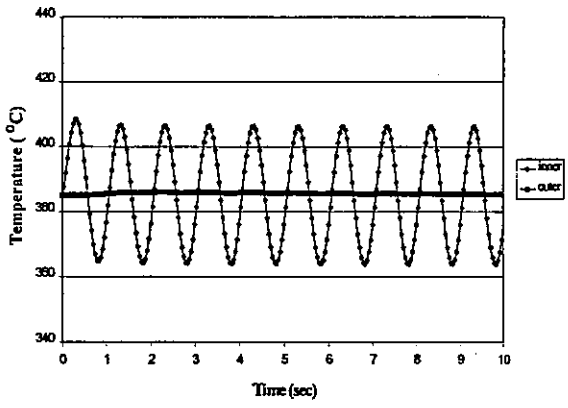

Fig.4f Temperature histories on the surfaces (1.0Hz)

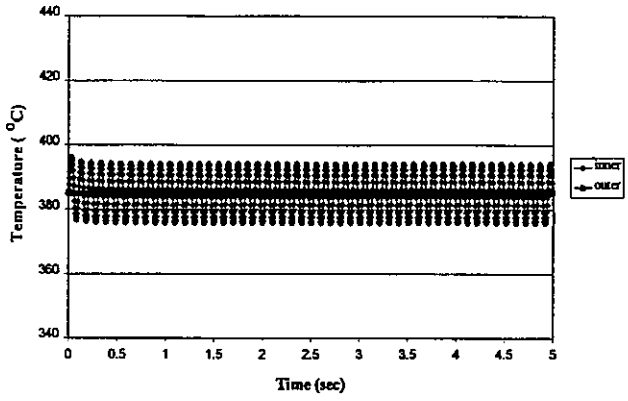

Fig.4g Temperature histories on the surfaces (10Hz)

Table 1 Temperature amplitude and difference between the both surfaces

Frequency value (Hz)	0.01	0.03	0.07	0.0846	0.1	1	10
(Tin-Tout)max	15.555	31.986	38.179	38.296	38.26	20.784	9.198
Tinner at (Tin-Tout)max	402.845	414.441	416.129	418.402	417.771	406.197	394.262
Touter at (Tin-Tout)max	387.29	382.455	377.95	380.106	379.511	385.413	385.064

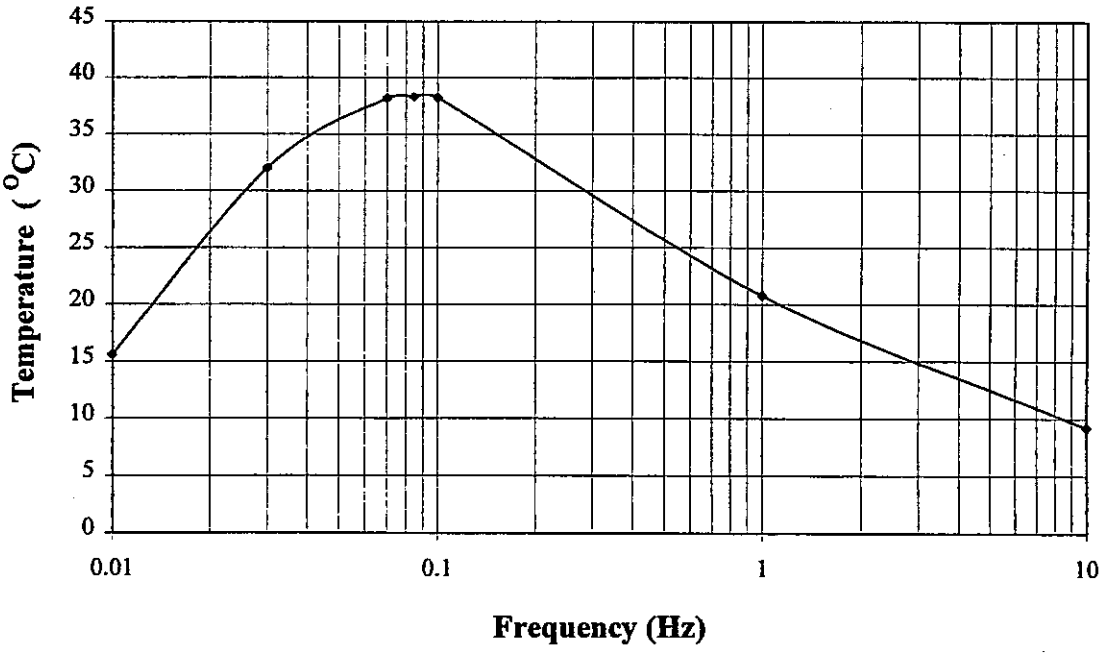

Fig.5 Maximum temperature difference between the inner and outer surfaces

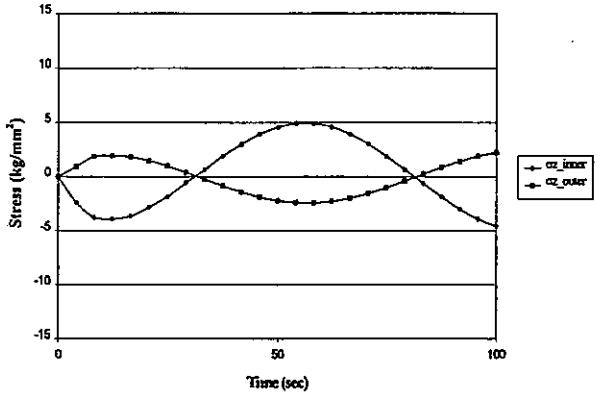

Fig.6a Stress histories on the surfaces (0.01Hz)

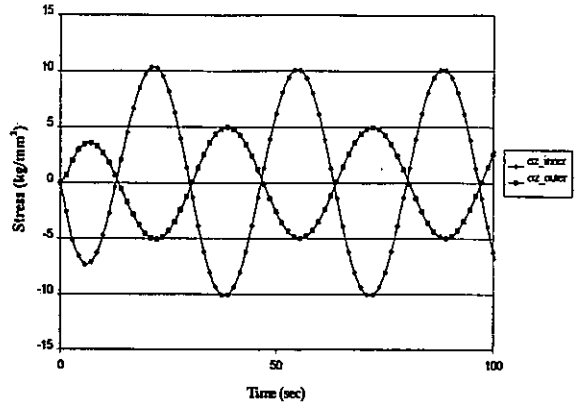

Fig.6b Stress histories on the surfaces (0.03Hz)

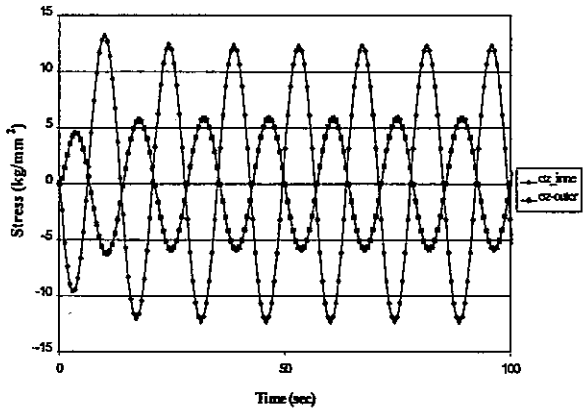

Fig.6c Stress histories on the surfaces (0.07Hz)

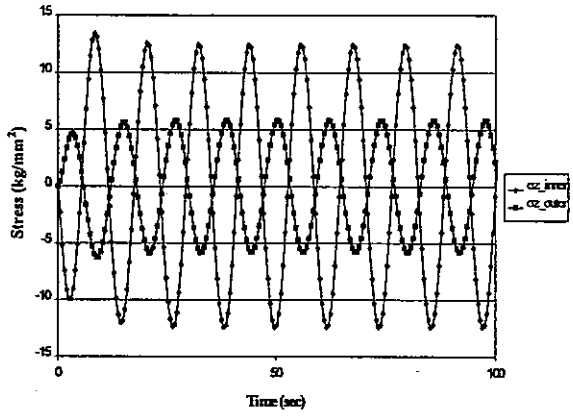

Fig.6d Stress histories on the surfaces (0.0846Hz)

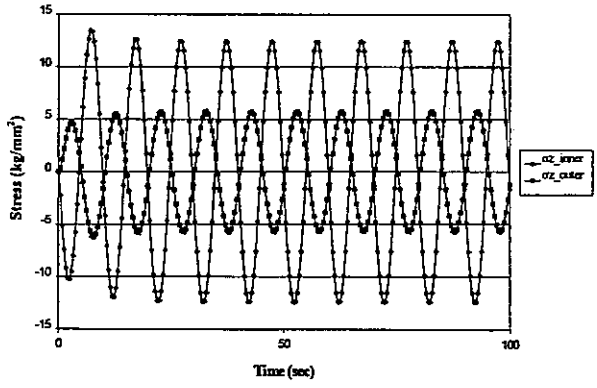

Fig.6e Stress histories on the surfaces (0.1Hz)

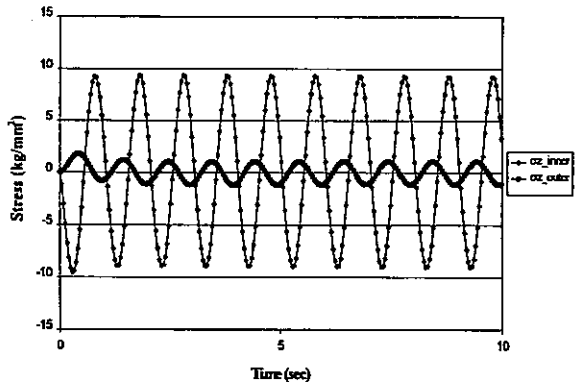

Fig.6f Stress histories on the surfaces (1.0Hz)

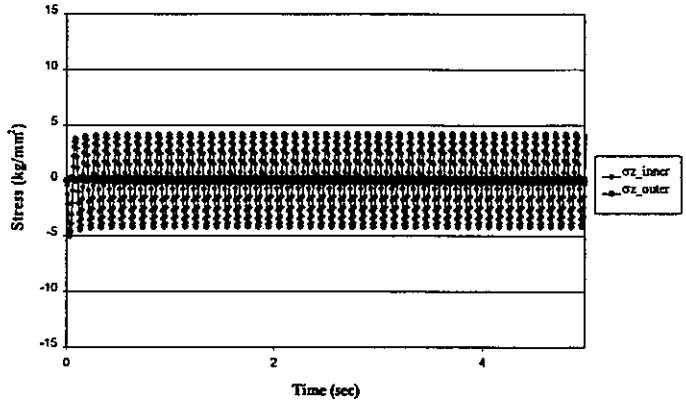

Fig.6g Stress histories on the surfaces (10Hz)

Table 2 Maximum and minimum stress at the inner surface

Frequency	σ z_inner (kg/mm²)			σ z(Mpa)
	σ z_max	σ z_min	σ z(max-min)	
0.01 Hz	4.89536	-4.8901	9.78548	95.897704
0.03 Hz	10.0711	-10.073	20.144	197.4112
0.07 Hz	12.2892	-12.296	24.5853	240.93594
0.0846 Hz	12.4131	-12.409	24.8219	243.25462
0.1 Hz	12.3972	-12.396	24.7927	242.96846
1.0 Hz	9.19692	-9.0471	18.244	178.791592
10 Hz	4.24517	-4.1713	8.41651	82.481798

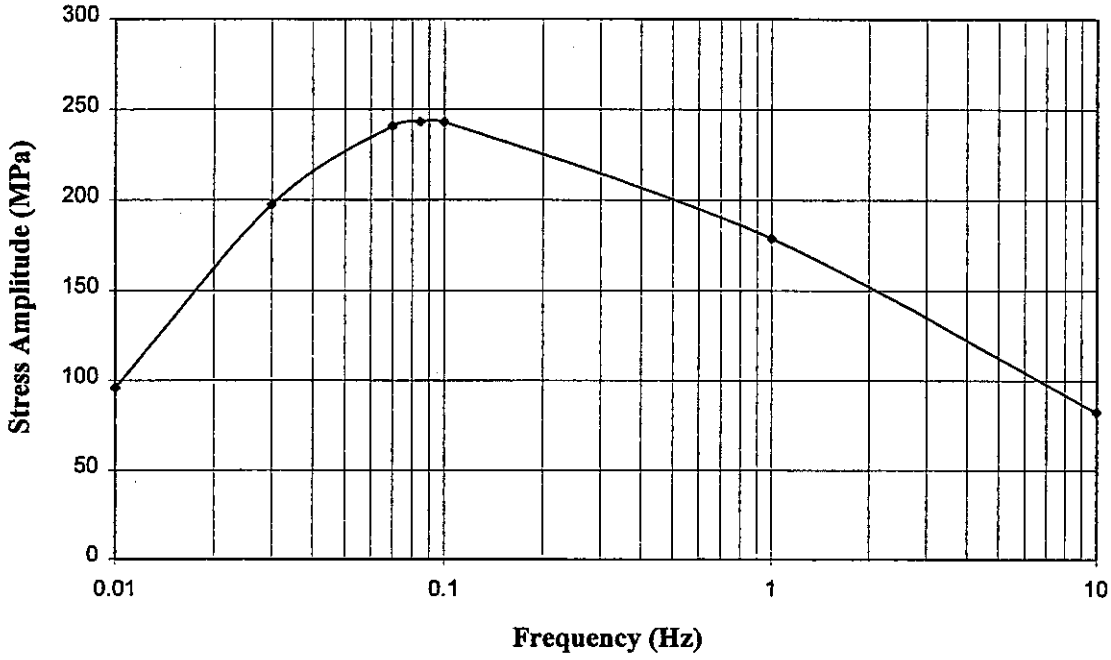

Fig.7 Stress amplitude induced by sinusoidal temperature fluctuation

3. Mechanism of structural responses to sinusoidal temperature fluctuations

In order to understand mechanism of structural responses to sinusoidal temperature fluctuations, theoretical approach is adopted to solve thermal and mechanical responses of a pipe wall due to sinusoidal temperature fluctuation shown in Fig.3.

In the case of thermal elastic problems under thermal transient, plates with the same wall thickness are fairly good approximation of thin pipes, where diameter is more than ten times than wall thickness[5]. To simplify formulation, let us introduce further approximation to evaluate thermal responses of thin pipes with the parts of a semi-infinite solid within distance of wall thickness from the surfaces. Accuracy of this approximation will be examined in the later. For a semi-infinite solid, 1-D heat conduction equation is described as

$$\frac{\partial T}{\partial t} = \frac{\lambda}{\rho c}\frac{\partial^2 T}{\partial x^2} \tag{2}$$

where T is ttemperature, t is time, λ is thermal conductivity, c is specific heat, and ρ is density. When temperature at a surface of a semi-infinite solid is due to sinusoidal fluctuation as in Fig.8a, boundary condition is

$$T_f = T|_{x=0} = \frac{1}{2}\Delta T_f \sin(\omega t) \tag{3}$$

where ΔT_f is amplitude of fluid temperature fluctuation, and ω is rotational frequency. Theoretical solutions of temperature in a semi-finite solid is[6]

$$T_s = T(x,t) = \frac{1}{2}\Delta T_f e^{-kx}\sin(\omega t - kx)\,, \tag{4}$$

where T_s is temperature of structures as a function of distance x from the surface and time t, $k = \sqrt{\frac{\omega}{2a}}$, $a = \frac{\lambda}{c\rho}$.

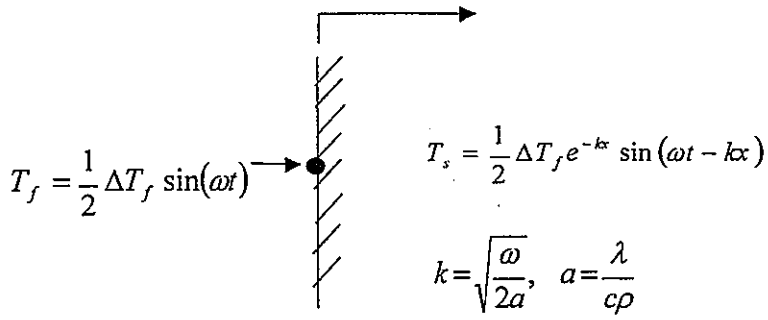

λ : Thermal conductivity, c: Specific heat, ρ : Density

Fig.8a Thermal response of a semi-infinite solid to sinusoidal temperature fluctuation on the surface

When heat flux into the surface of a semi-infinite solid fluctuates in sinusoidal way as in Fig.8b, boundary condition becomes

$$q_0 = -\lambda \left.\frac{\partial T}{\partial x}\right|_{x=0} = \frac{1}{2} A \sin(\omega t), \tag{5}$$

where A is amplitude of heat flux fluctuation.

Theoretical solutions of temperature in a semi-finite solid [6] is

$$T_s = T(x,t) = \frac{A}{2\sqrt{2}\lambda k} e^{-kx} \sin\left(\omega t - kx - \frac{\pi}{4}\right). \tag{6}$$

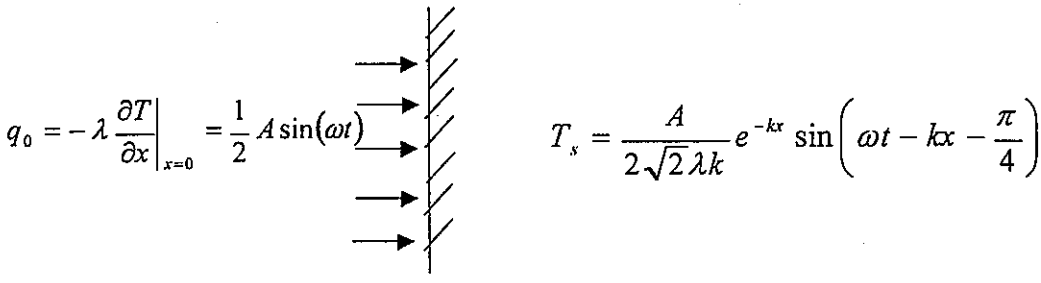

Fig.8b Thermal Response of a Semi-infinite Solid to Sinusoidal heat flux fluctuation on the surface

When fluid temperature fluctuates in sinusoidal way and is transferred to a surface of a semi-infinite solid with a constant heat-transfer coefficient as in Fig.8c, boundary condition is

$$-\lambda \left.\frac{\partial T}{\partial x}\right|_{x=0} = h(T|_{x=0} - T_f), \quad T_f = \frac{1}{2}\Delta T_f \sin(\omega t), \tag{7}$$

where h is heat-transfer coefficient.

Theoretical solutions of temperature in a semi-finite solid[6] is

$$T_s = T(x,t) = \frac{1}{2}\Delta T_s e^{-kx} \sin(\omega t - kx - \varepsilon), \tag{8}$$

where amplitude of structural temperature fluctuation is $\Delta T_s = \dfrac{\Delta T_f h^*}{\sqrt{(h^*+k)^2 + k^2}}$,

$h^* = \dfrac{h}{\lambda}$, and $\varepsilon = \tan^{-1}\left[k/(h^*+k)\right]$.

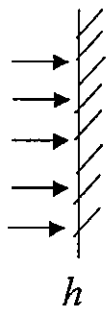

$$T_f = \frac{1}{2}\Delta T_f \sin(\omega t) \qquad T_s = \frac{\Delta T_f h^*}{2\sqrt{(h^*+k)^2 + k^2}} e^{-kx} \sin(\omega t - kx - \varepsilon)$$

$$h^* = \frac{h}{\lambda} \qquad \varepsilon = \tan^{-1}\left[k/(h^*+k)\right]$$

h: Heat-transfer coefficient

Fig.8c Thermal response of a semi-infinite solid to sinusoidal temperature fluctuation of fluid with heat convection

The case of Fig.8c is the closest condition to thermal striping phenomena. When substituting the material properties of Type304SS, fluid temperature amplitude 251℃(Maximum Temperature:381℃, Minimum Temperature:130℃), and coefficient of heat transfer 8.8517x10-6 kcal/mm2 *sec*℃ into Eq.(8), temperature profiles in a semi-infinite solid due to sinusoidal temperature fluctuation with the various frequencies can be calculated as in Fig.9. The important point from these results is that

temperature amplitude is reduced monotonously when frequency becomes high. This trend can be explained by Eq.(8), where a term of amplitude of structural temperature fluctuation ΔT_s contains frequency in a denominator. Its phisical meaning is considered as attenuation factors by non-stationary heat transfer in Fig.1.

By using temperature distribution derived from Eq.(8), induced thermal stress distribution $\sigma(x,t)$ can be quantitatively evaluated by thermal elastic theory on plates as

$$\begin{aligned}\sigma(x,t) &= \frac{E\alpha}{1-\nu}\left\{T_s(x,t)-\frac{1}{L}\int_0^L T_s(x,t)dx\right\} \\ &= \frac{E\alpha\Delta T_s}{2(1-\nu)}\left\{e^{-kx}\sin(\omega t-kx-\varepsilon)-\frac{1}{L}\int_0^L e^{-kx}\sin(\omega t-kx-\varepsilon)dx\right\} \\ &= \frac{E\alpha\Delta T_s}{2(1-\nu)}\left[e^{-kx}\sin(\omega t-kx-\varepsilon)+\frac{1}{\sqrt{2}kL}\left\{e^{-kL}\sin\left(\omega t-kL-\varepsilon-\frac{\pi}{4}\right)-\sin\left(\omega t-\varepsilon-\frac{\pi}{4}\right)\right\}\right],\end{aligned} \tag{9}$$

where $\Delta T_s = \dfrac{\Delta T_f h^*}{\sqrt{(h^*+k)^2+k^2}}$.

From Eq.(9), stress amplitude is a function of heat convection, frequency, wall thickness, thermal conductivity, specific heat, density, Young's modulus, and thermal expansion ratio.

Eq.(9) also explains us that thermal stress is caused by temperature deviation of evaluation points from average temperature of wall thickness. In the case of very low frequency of fluctuation or thin wall thickness, since heat conduction in the wall thickness, average temperature can follow temperature change of evaluation points, therefore thermal stress is mitigated. It is the attenuation factors from thermal unloading in Fig.1.

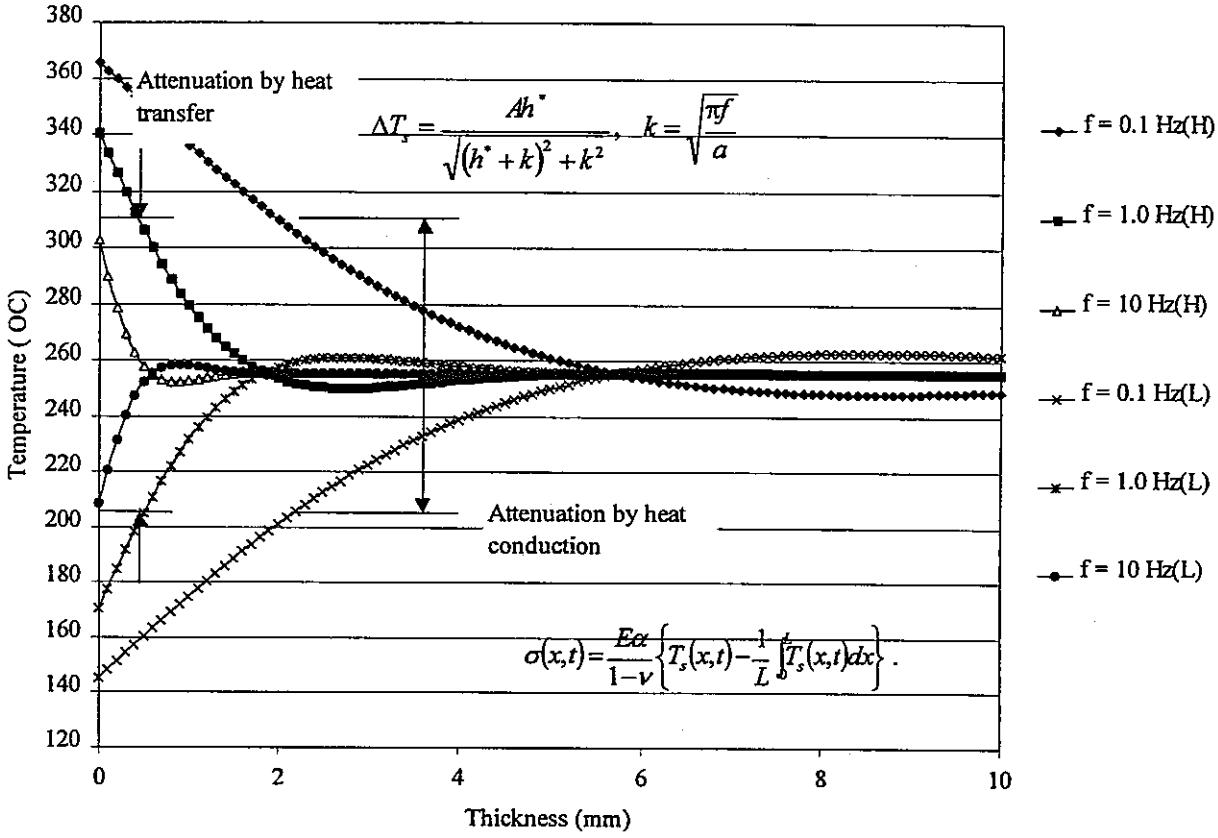

Fig.9 Temperature profile in a semi-infinite solid due to sinusoidal temperature fluctuation

4. Non-dimensional structural response diagram (NSRD)

Since Eq.(9) is a complicated equation with many parameters for specific cases, more general equations and diagrams will be derived for adoption to design use, by introduction of the following non-dimensional parameters:

Biot Number $Bi = \frac{hL}{\lambda}$, (10)

Fourier Number $t^* = \frac{ta}{L^2}$, (11)

Non-dimensional frequency defined by $f^* = \frac{fL^2}{a}$, (12)

which is proposition of this study,

Non-dimensional thermal stress defined by $\sigma^* = \sigma|_{x=0} / \frac{E\alpha\Delta T_f}{1-\nu}$, (13)

which means the ratio of actual thermal stress to ideal thermal stress caused from 100% of fluid temperature amplitude, and are defined between zero and one.

By substituting Eqs.(10) – (13) to Eq.(9), non-dimensional stress at the inner surface (x=0) is

$$\sigma^* = \frac{1}{2} H(B_i, f^*) \Lambda(f^*, t^*), \tag{14}$$

where $$H(B_i, f^*) = \frac{B_i}{\sqrt{\left(B_i + \sqrt{\pi f^*}\right)^2 + \pi f^*}}, \tag{15}$$

$$\Lambda(B_i, f^*, t^*) = \sin(2\pi f^* t^* - \varepsilon^*) + \frac{1}{\sqrt{2\pi f^*}} \left\{ e^{-\sqrt{\pi f^*}} \sin\left(2\pi f^* t^* - \sqrt{\pi f^*} - \varepsilon^* - \frac{\pi}{4}\right) - \sin\left(2\pi f^* t^* - \varepsilon^* - \frac{\pi}{4}\right) \right\}, \tag{16}$$

and $\varepsilon^* = \tan^{-1}\left[\sqrt{\pi f^*} / \left(Bi + \sqrt{\pi f^*}\right)\right]$.

Since phase delay has no influence on stress amplitude and can be neglected, Eqs. (14)-(16) can be reduced to,

$$\sigma^* = \frac{1}{2} H(B_i, f^*) \Lambda(f^*, t^*) \tag{17}$$

where $H(B_i, f^*) = \dfrac{B_i}{\sqrt{\left(B_i + \sqrt{\pi f^*}\right)^2 + \pi f^*}}$, (18)

which is attenuation factor by non-stationary heat transfer, and

$$\Lambda(f^*, t^*) = \sin(2\pi f^* t^*) + \frac{1}{\sqrt{2\pi f^*}} \left\{ e^{-\sqrt{\pi f^*}} \sin\left(2\pi f^* t^* - \sqrt{\pi f^*} - \frac{\pi}{4}\right) - \sin\left(2\pi f^* t^* - \frac{\pi}{4}\right) \right\}, \tag{19}$$

which is attenuation factor by thermal unloading.

By using Eqns.(17)-(19), relationship between amplitude of non-dimensional thermal stress $\Delta\sigma^*$ and non-dimensional frequency f^* were calculated for the different Biot number B_i as in Fig.10, which is named the Non-dimensional structural response diagram (NSRD).

Definition of a heat-transfer coefficient is difficult for the thermal striping problem since this value is actually non-stationary during fluctuation. R&Ds for a heat-transfer problem between fluid and structure under thermal striping phenomenon are required to determine rational Biot number for the NSRD.

$$\sigma^* = \frac{1}{2} H(B_i, f^*) N(f^*, t^*)$$

$$H(B_i, f^*) = \frac{B_i}{\sqrt{\left(B_i + \sqrt{\pi f^*}\right) + \pi f^*}}$$

③Non-stationary Heat Convection

$$N(f^*, t^*) = \sin(2\pi f^* t^*) + \frac{1}{\sqrt{2\pi f^*}} \left\{ e^{\sqrt{\pi f^*}} \sin\left(2\pi f^* t^* - \sqrt{\pi f^*} - \frac{\pi}{4}\right) - \sin\left(2\pi f^* t^* - \frac{\pi}{4}\right) \right\}$$

④Thermal Unloading

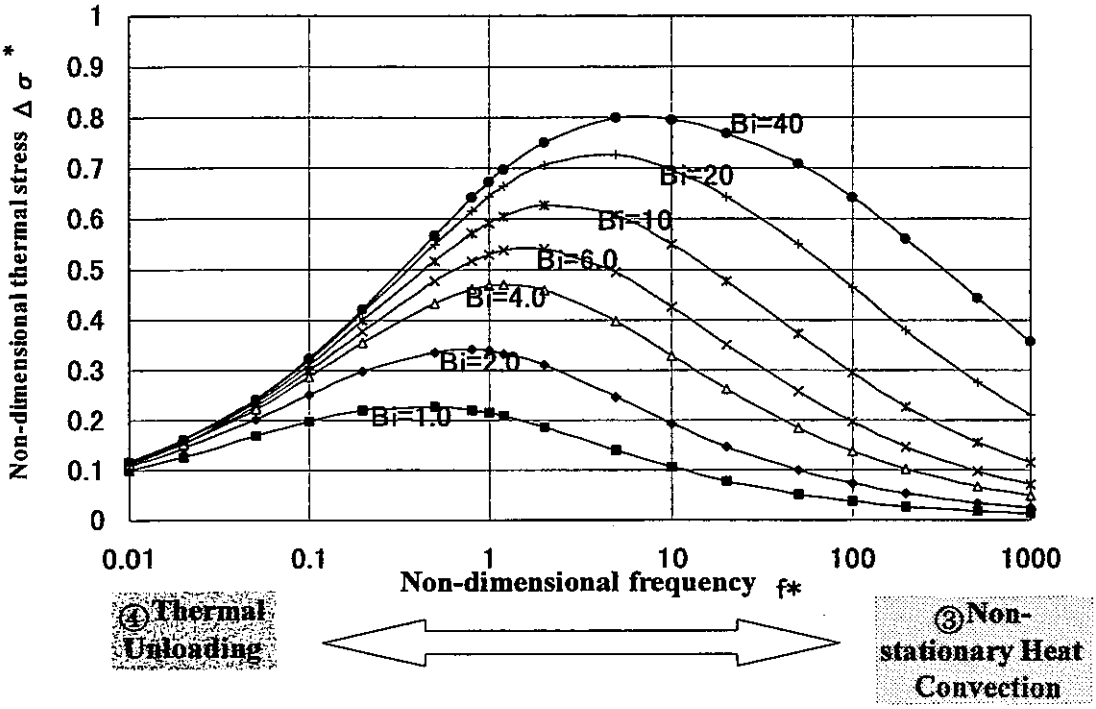

Fig.10 Non-dimensional Structural Response Diagram (NSRD)

5. Verification of Non-dimensional structural response diagram

5.1 Finite element calculation

Accuracy of the derived NSRD under assumption of 1-D heat conduction of a semi-infinite solid will be verified through comparison with F.E. calculated results. Structural responses of the pipe wall due to sinusoidal fluid temperature were calculated by FINAS code and were plotted in the NSRD.

Analysis conditions were almost the same as the case of Phenix shown in Fig.3 and different points from the original problem are as follows. Wall thickness was changed to 1.049553 mm, 6.297319 mm, and 41.98213 mm for control of Biot nuber. Suitable frequencies of temperature fluctuation were selected to plot structural response diagrams.

F.E. calculated results from the analysis cases tabulated in Table 3 gave relationships between amplitude of non-dimensional thermal stress $\Delta\sigma^{*}=\Delta\sigma/\Delta\sigma_{max}(\Delta T_f)$ and non-dimensional frequency f* as in Table 4 and Fig.11, where $\Delta\sigma = \Delta\sigma_z = \Delta\sigma_\theta$, $\Delta\sigma_{max}(\Delta T_f) = E\alpha\Delta T_f/(1-\upsilon)$. Let us call Non-dimensional structural response diagram obtained from F.E. calculation as the numerical NSRD.

Table 3 Analysis Cases

Bi* = 1.0		Bi* = 6.0		Bi* = 40	
Thickness = 1.049553 mm		Thickness = 6.297319 mm		Thickness = 41.98213 mm	
f*	frequency (Hz)	f*	frequency (Hz)	f*	frequency (Hz)
0.01	0.037792845	0.01	0.001049801	0.01	2.36205E-05
0.02	0.075585689	0.02	0.002099602	0.02	4.72411E-05
0.05	0.188964223	0.05	0.005249006	0.05	0.000118103
0.1	0.377928446	0.1	0.010498012	0.1	0.000236205
0.2	0.755856892	0.2	0.020996025	0.2	0.000472411
0.5	1.889642229	0.5	0.052490062	0.5	0.001181026
0.8	3.023427566	0.8	0.083984099	0.8	0.001889642
1	3.779284458	1	0.104980124	1	0.002362053
1.2	4.53514135	1.2	0.125976149	1.2	0.002834463
2	7.558568916	2	0.209960248	2	0.004724106
5	18.89642229	5	0.524900619	5	0.011810264
10	37.79284458	10	1.049801238	10	0.023620528
20	75.58568916	20	2.099602477	20	0.047241056
50	188.9642229	50	5.249006192	50	0.118102639
100	377.9284458	100	10.49801238	100	0.236205279
200	755.8568916	200	20.99602477	200	0.472410557
500	1889.642229	500	52.49006192	500	1.181026393
1000	3779.284458	1000	104.9801238	1000	2.362052786

*Bi : Biot number ($Bi = hl/\lambda$)

Table 4 Sinusoidal Analysis Results

f*	Bi = 1.0			Bi = 6.0			Bi = 40		
	f(Hz)	Δσ(kg/mm)	$\Delta\sigma/\Delta\sigma_{max}(\Delta T_f)$	f(Hz)	Δσ(kg/mm)	$\Delta\sigma/\Delta\sigma_{max}(\Delta T_f)$	f(Hz)	Δσ(kg/mm)	$\Delta\sigma/\Delta\sigma_{max}(\Delta T_f)$
0.01	0.03779284	0.886072	0.02089188	0.0010498	0.901409	0.021253497	2.3621E-05	0.963946	0.022728
0.02	0.07558569	1.754549	0.041368903	0.0020996	1.795872	0.04234322	4.7241E-05	1.923075	0.045342423
0.05	0.18896422	4.08312	0.096272145	0.00524901	4.43071	0.104467652	0.0001181	4.73953	0.111749035
0.1	0.37792845	6.77246	0.159681629	0.01049801	8.48325	0.200018779	0.00023621	9.26805	0.218522859
0.2	0.75585689	8.9634	0.211339796	0.02099602	14.67172	0.345931044	0.00047241	16.72791	0.394412064
0.5	1.88964223	9.88635	0.233101189	0.05249006	22.1716	0.522763843	0.00118103	27.4708	0.647708824
0.8	3.02342757	9.69963	0.228698689	0.0839841	23.8714	0.562841869	0.00188964	30.6424	0.722489075
1	3.77928446	9.445	0.222695001	0.10498012	24.0873	0.567932378	0.00236205	31.703	0.74749599
1.2	4.53514135	9.2137	0.217241391	0.12597615	24.1095	0.568455811	0.00283446	32.3552	0.762873617
2	7.55856892	8.08312	0.190584481	0.20996025	23.6833	0.558406832	0.00472411	33.2135	0.783110686
5	18.8964223	5.85767	0.138112634	0.52490062	20.8535	0.49168557	0.01181026	34.0391	0.802576752
10	37.7928446	4.43149	0.104486043	1.04980124	17.87464	0.42144976	0.02362053	33.7608	0.796014971
20	75.5856892	3.28139	0.077368888	2.09960248	14.75416	0.347874821	0.04724106	32.4902	0.766056658
50	188.964223	2.18026	0.051406353	5.24900619	10.80204	0.254691404	0.11810264	29.8777	0.704458914
100	377.928446	1.573863	0.037108674	10.4980124	8.20727	0.1935117	0.23620528	26.9998	0.636603547
200	755.856892	1.130936	0.026665304	20.9960248	6.1051	0.143946559	0.47241056	23.4359	0.552573614
500	1889.64223	0.731602	0.017249773	52.4900619	4.10105	0.096694901	1.18102639	18.56819	0.43780234
1000	3779.28446	0.533233	0.012572612	104.980124	3.05408	0.072009354	2.36205279	15.26523	0.359924872

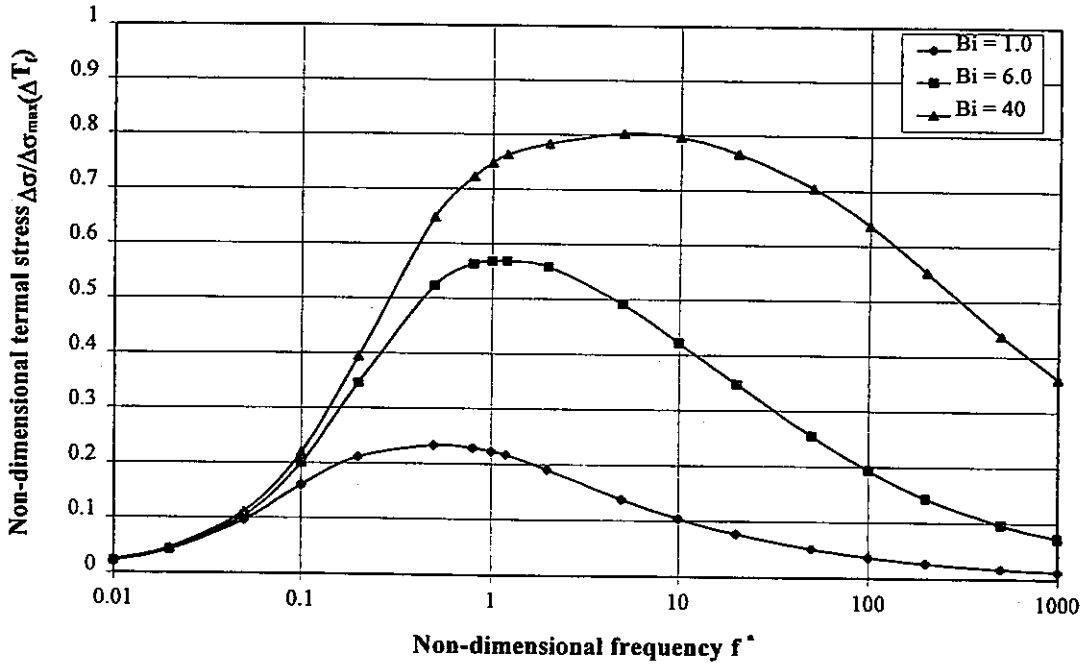

Fig.11 Numerical Non-dimensional structural response diagram

5.2 Comparison of theoretical NSRD with numerical NSRD

The same problem as in Table 3 was predicted by Eqns.(17)-(19), which was named as a theoretical NSRD to distinguish from numerical one, and was over plotted into Fig.11 as in Fig.12.

What are evident from Fig.12 are follow. Numerical NSRD is similar to theoretical NSRD, when non-dimensional frequency is high. Stresses of theoretical NSRD are larger than ones of Numerical NSRD, in low frequency region. In the case that Biot number is 6.0 and 40, stresses of Numerical NSRD are higher than ones of theoretical NSRD, when non-dimensional frequency is between 0.5 and 2.0.

We extend our investigations of the reason why both diagrams have slight differences. Fig.13 shows the comparisons of temperature amplitude at the inner and outer surface between FEM and 1-D theory. Fig.14-Fig.16 show the comparisons of temperature distribution across wall thickness when the temperature of the inner surface is the maximum and the minimum between non-dimensional structural response diagram based on finite element analysis and on 1-D theory when Biot number is 1.0, 6.0 and 40. Fig.17-Fig.19 show the comparisons of stress distribution across wall thickness between finite element analysis and 1-D theory, when Biot number is 1.0, 6.0 and 40. Fig.20-Fig.21 show the temperature histories at the inner and the outer surface based on finite element analysis under non-dimensional frequency f* is 0.01, 0.1, 0.2, 0.5, 0.8, 1.0, 1.2, and 2.0, when Biot number is 6.0 and 40. Temperature amplitude on the both surface becomes large, when non-dimensional frequency f* is low.

From above results, we can draw a conclusion as follows. Numerical NSRD is similar to theoretical NSRD, when non-dimensional frequency is high, since both temperature of the inner surface is the same and average temperature of the wall is approximately the constant, which is as same as intermediate of the maximum and the minimum temperature of temperature fluctuation.

On the other hand, Stresses of theoretical NSRD are larger than ones of Numerical NSRD, in low frequency region, because the theoretical inner surface temperature is close to numerical one, however, amplitude of theoretical calculated average temperature of the wall is larger than numerical one when non-dimensional frequency is low.

In the case that Biot number is 6.0 and 40, stresses of Numerical NSRD are higher than ones of theoretical NSRD, when non-dimensional frequency is in the range between 0.5 and 2.0. In this case, the inner surface temperature is approximately the same between numerical and theoretical one, however, amplitude of theoretical calculated average temperature of the wall is larger than numerical one. The reason why amplitude of theoretical average temperature becomes large is considered to be differences of temperature profiles in the range between 0.5 and 2.0 from Fig.15 and Fig.16.

When rearranging above results, theoretical NSRD can approximate and almost can bound

numerical NSRD conservatively. In the case that Biot number is 6.0 and 40, stresses of Numerical NSRD are higher than ones of theoretical NSRD within the error of 4.67 %. When adopting solution of temperature profiles of finite plates[7] instead of one of a semi-infinite solid, accuracy will be improved.

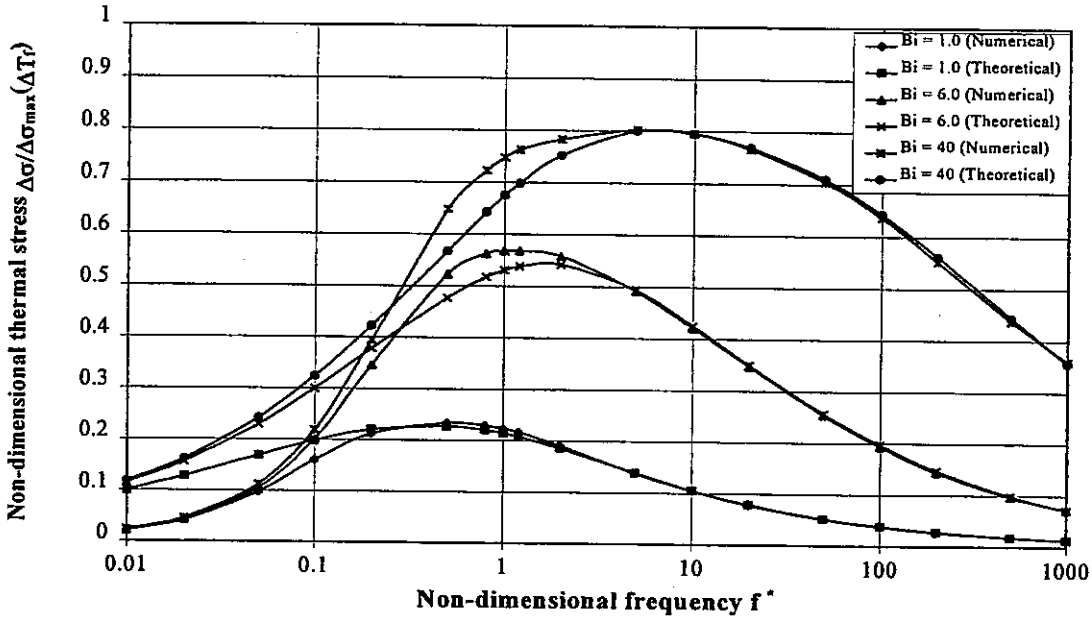

Fig.12 Comparisons of the numerical and the theoretical Non-dimensional structural response diagrams

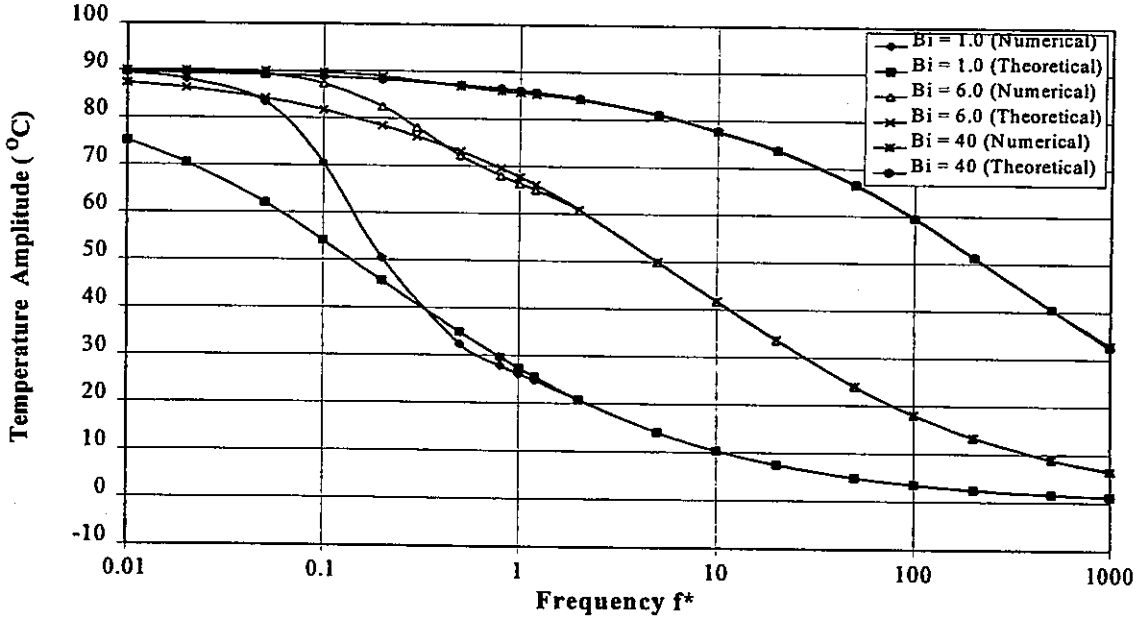

Fig.13a Comparisons of temperature amplitude on the inner surface between FEM and 1-D theory

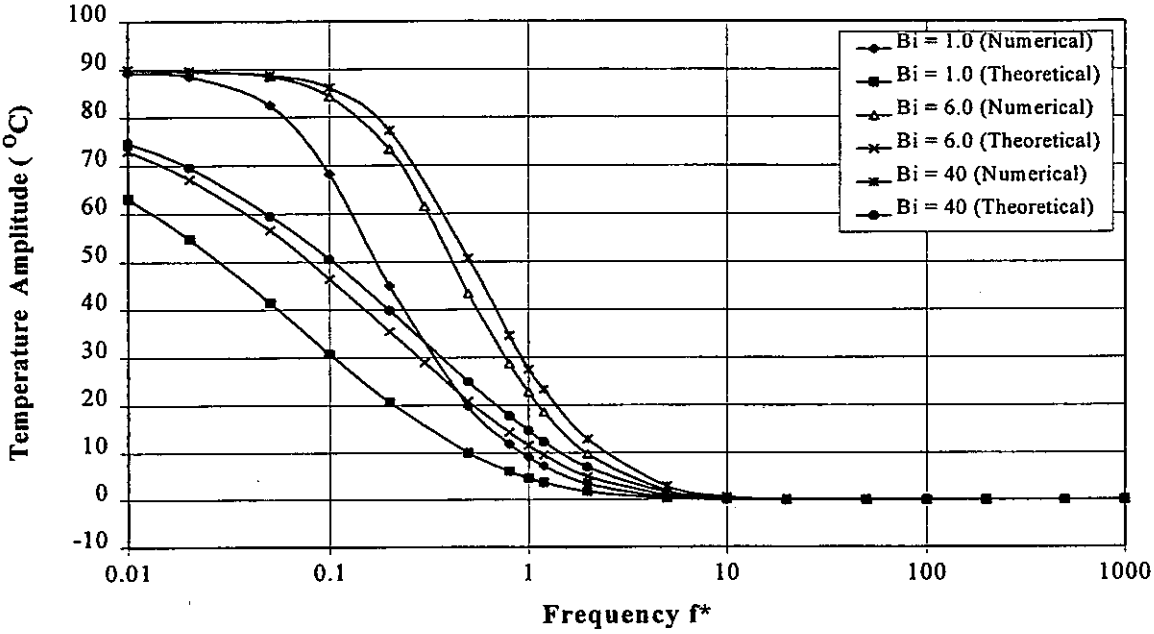

Fig.13b Comparisons of temperature amplitude on the outer surface between FEM and 1-D theory

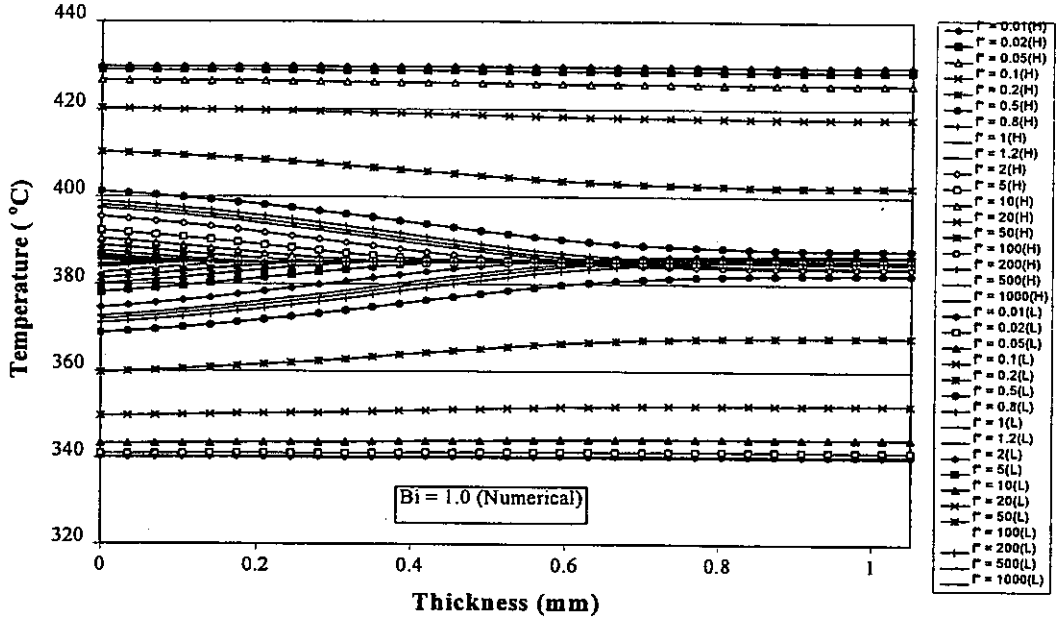

Fig.14a Numerical results of temperature distribution when inner surface temperature is the maximum(H) and the minimum(L) under Biot number = 1.0

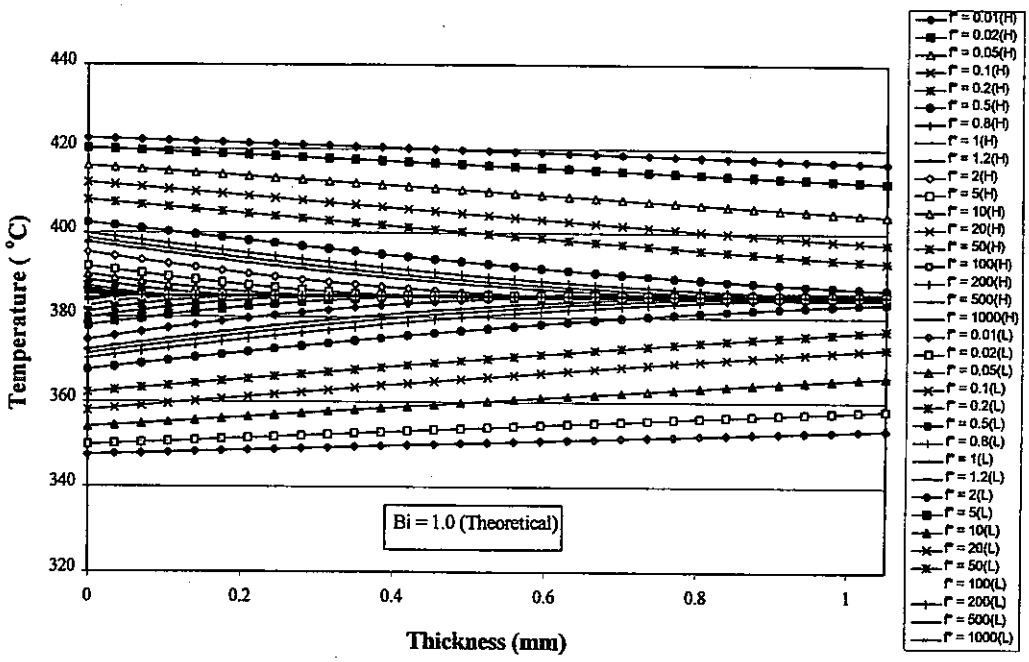

Fig.14b Theoretical results of temperature distribution when inner surface temperature is the maximum(H) and the minimum(L) under Biot number = 1.0

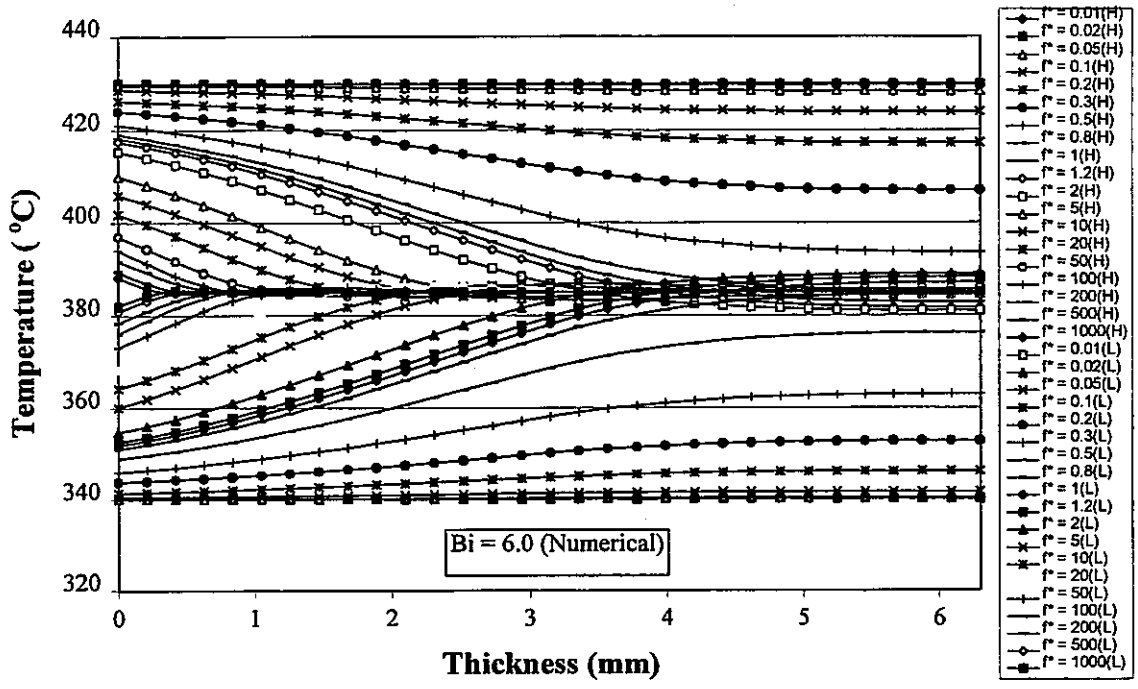

Fig.15a Numerical results of temperature distribution when inner surface temperature is the maximum(H) and the minimum(L) under Biot number = 6.0

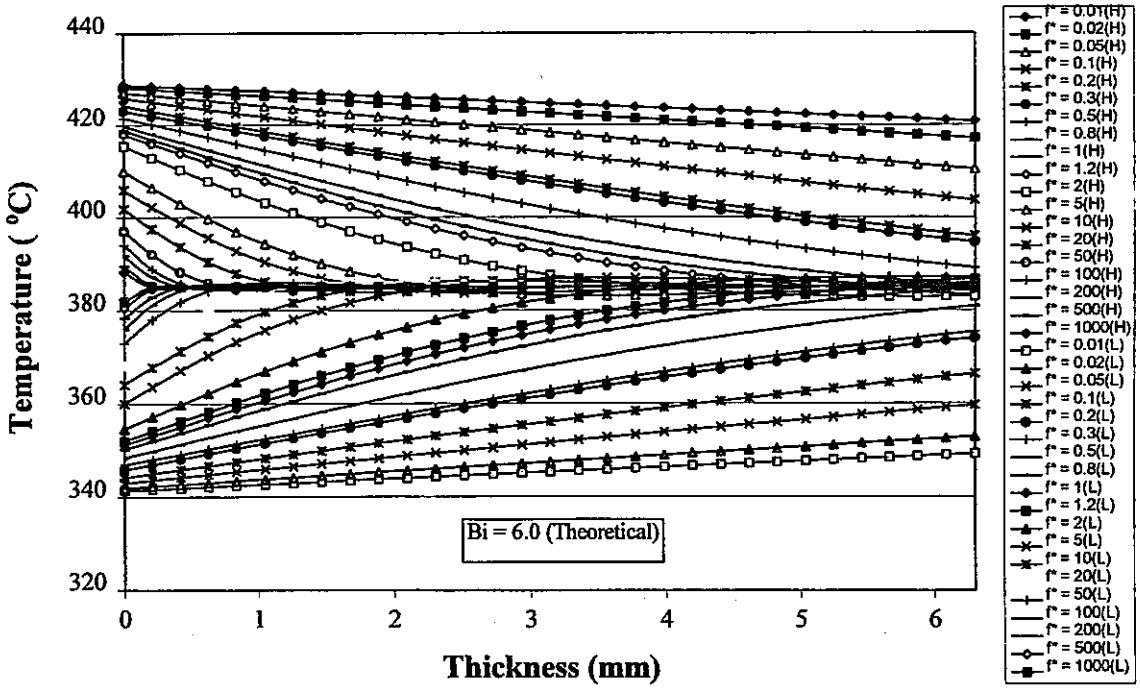

Fig.15b Theoretical results of temperature distribution when inner surface temperature is the maximum(H) and the minimum(L) under Biot number = 6.0

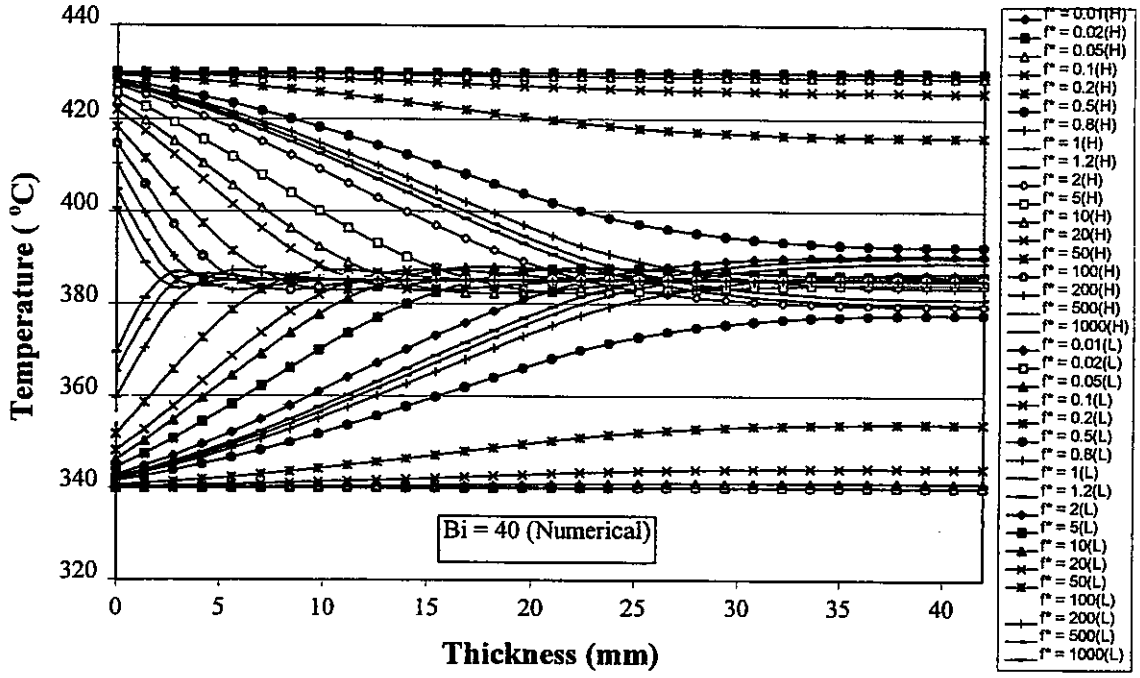

Fig.16a Numerical results of temperature distribution when inner surface temperature is the maximum(H) and the minimum(L) under Biot number = 40

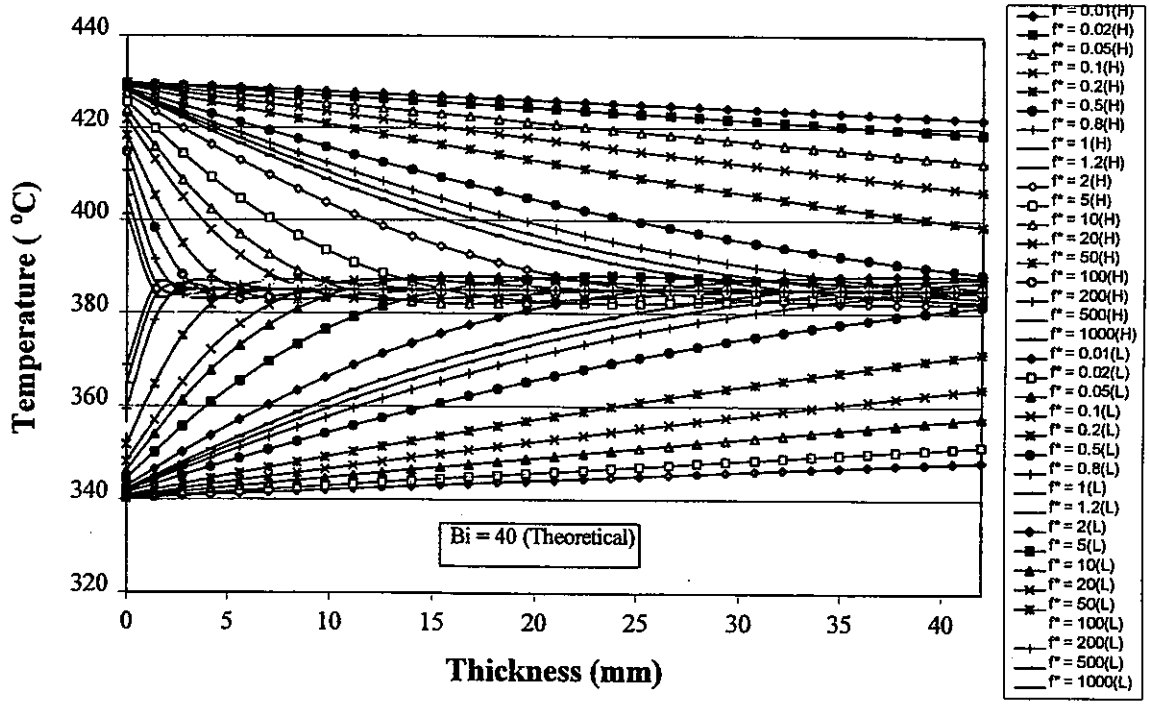

Fig.16b Theoretical results of temperature distribution when inner surface temperature is the maximum(H) and the minimum(L) under Biot number = 40

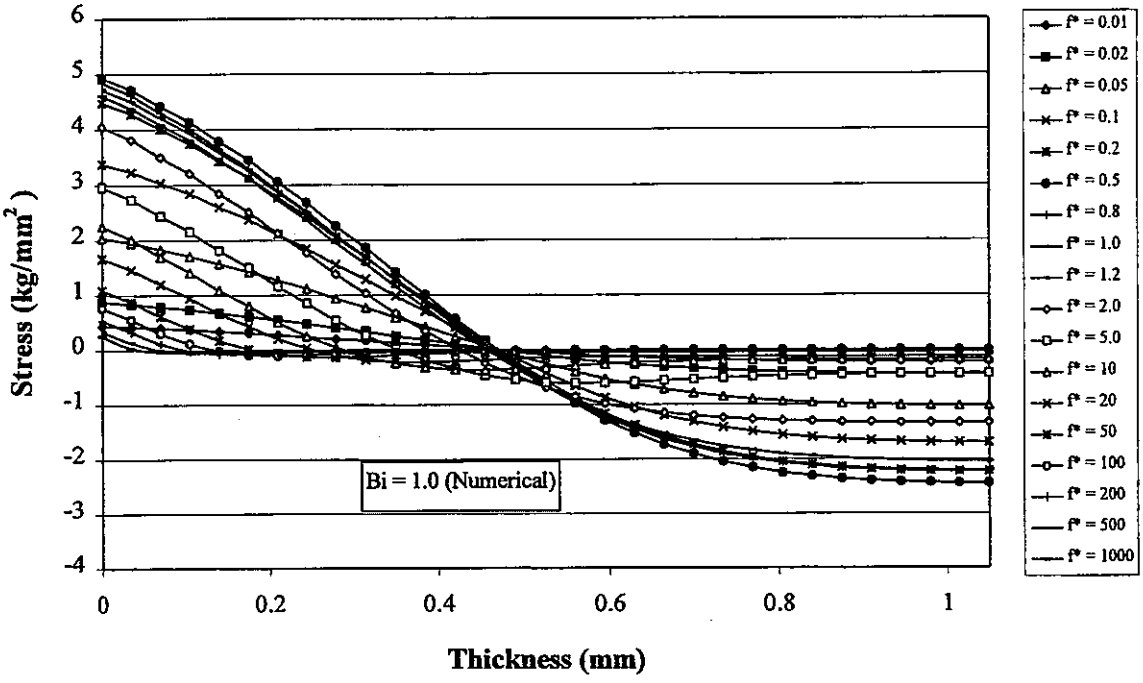

Fig.17a Numerical results of stress distribution across wall thickness when Bi = 1.0

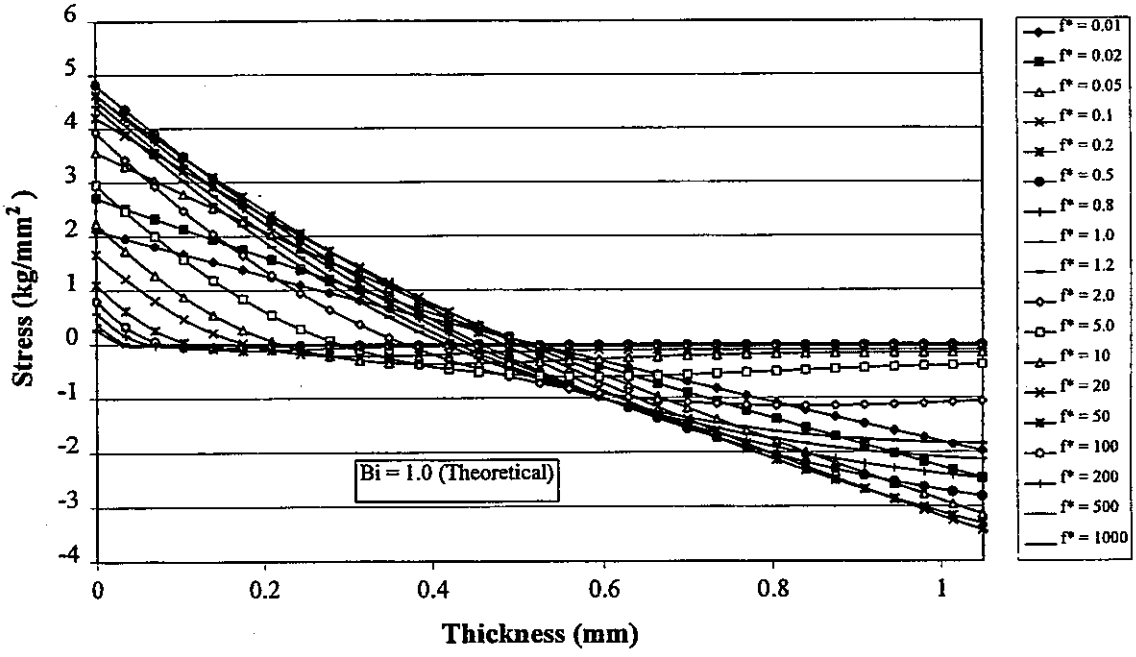

Fig.17b Theoretical results of stress distribution across wall thickness when Bi = 1.0

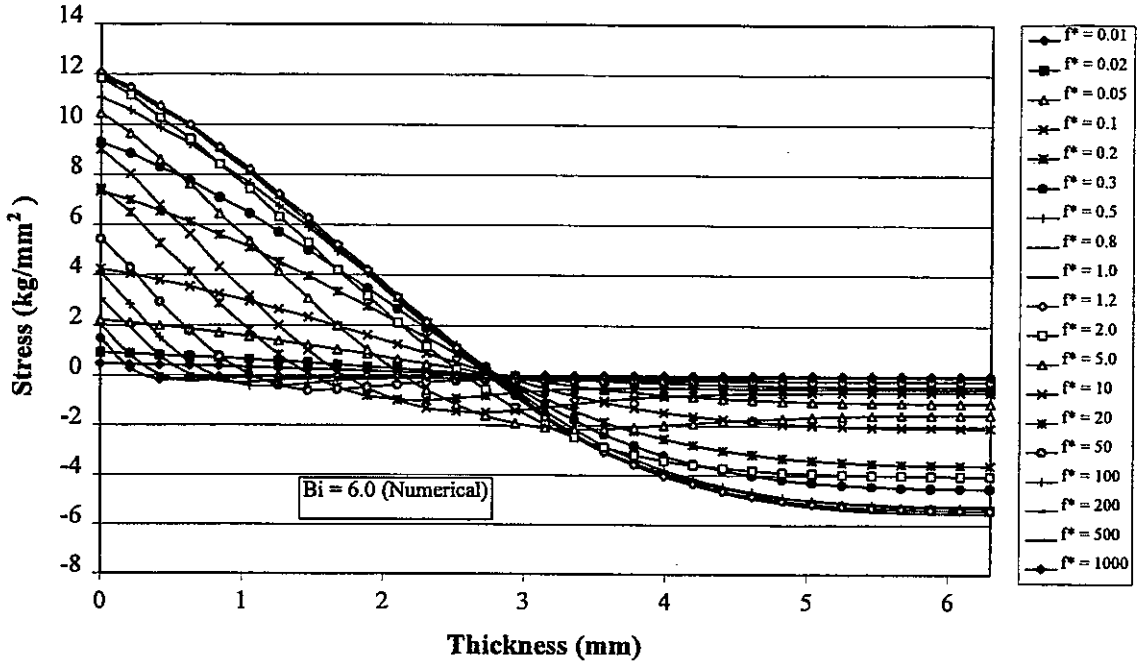

Fig.18a Numerical results of stress distribution across wall thickness when Bi = 6.0

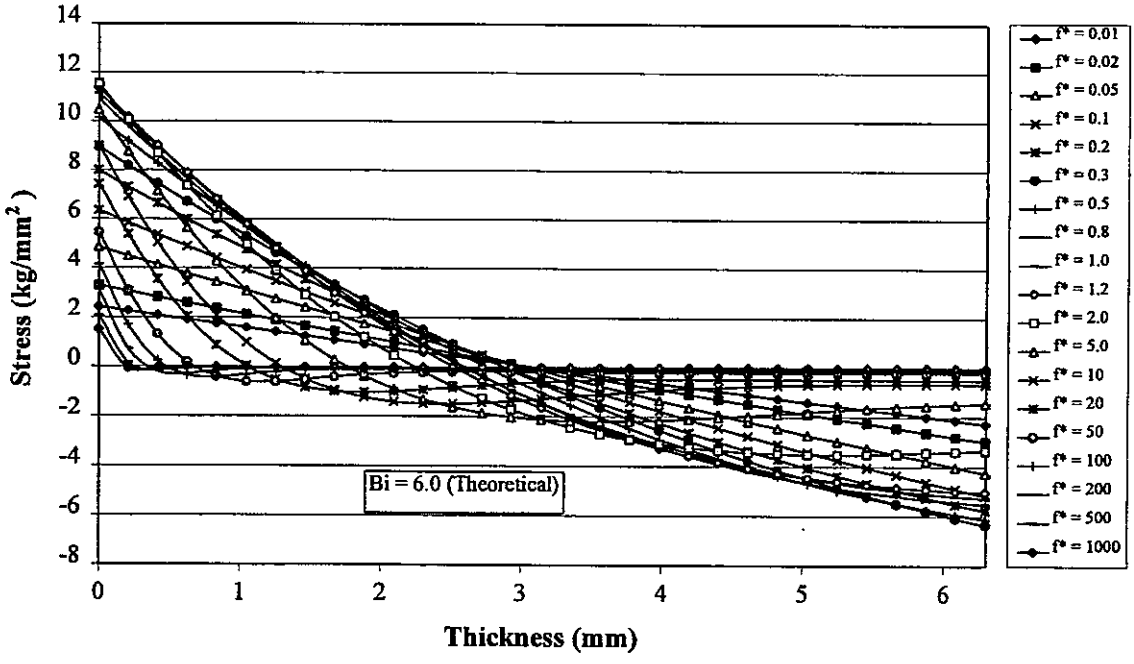

Fig.18b Theoretical results of stress distribution across wall thickness when Bi = 6.0

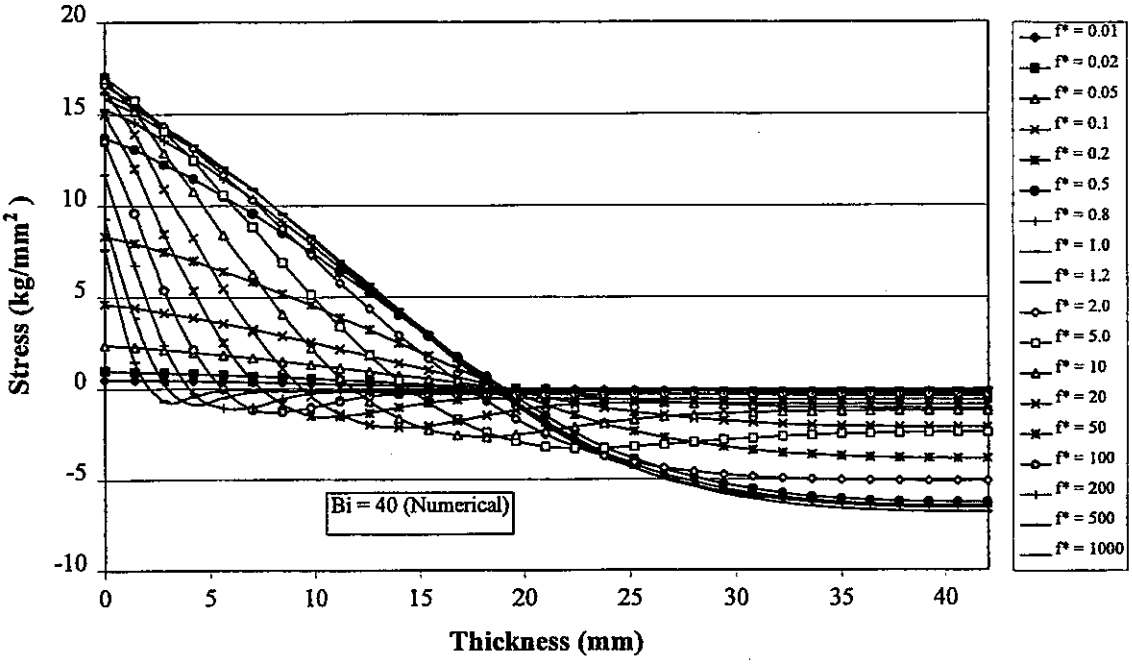

Fig.19a Numerical results of stress distribution across wall thickness when Bi = 40

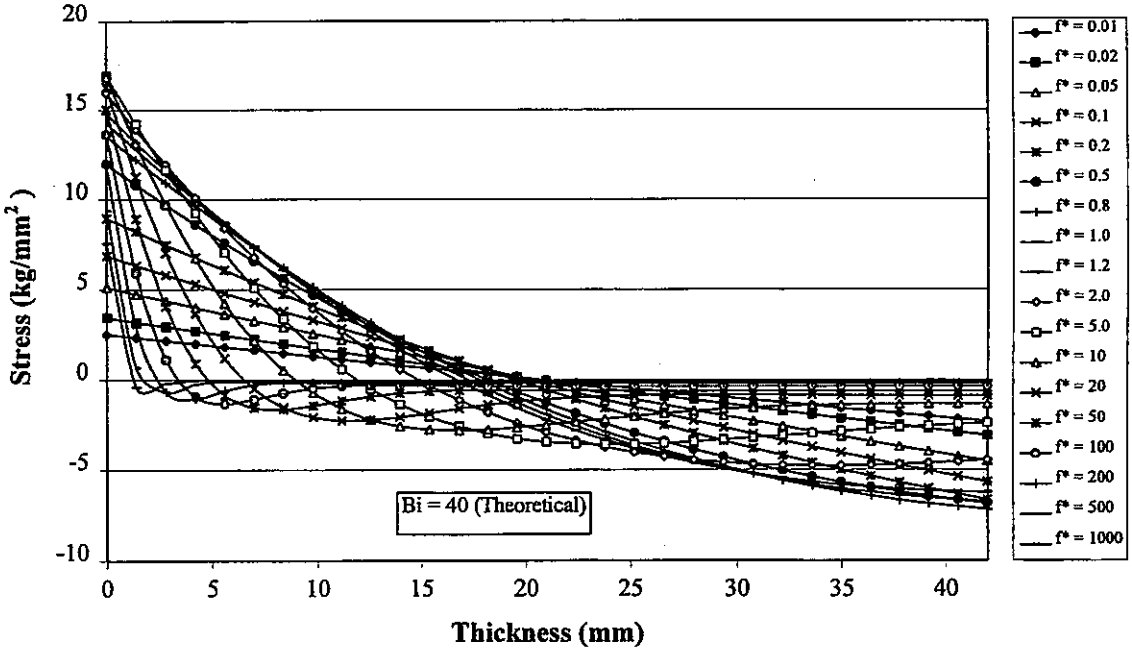

Fig.19b Theoretical results of stress distribution across wall thickness when Bi = 40

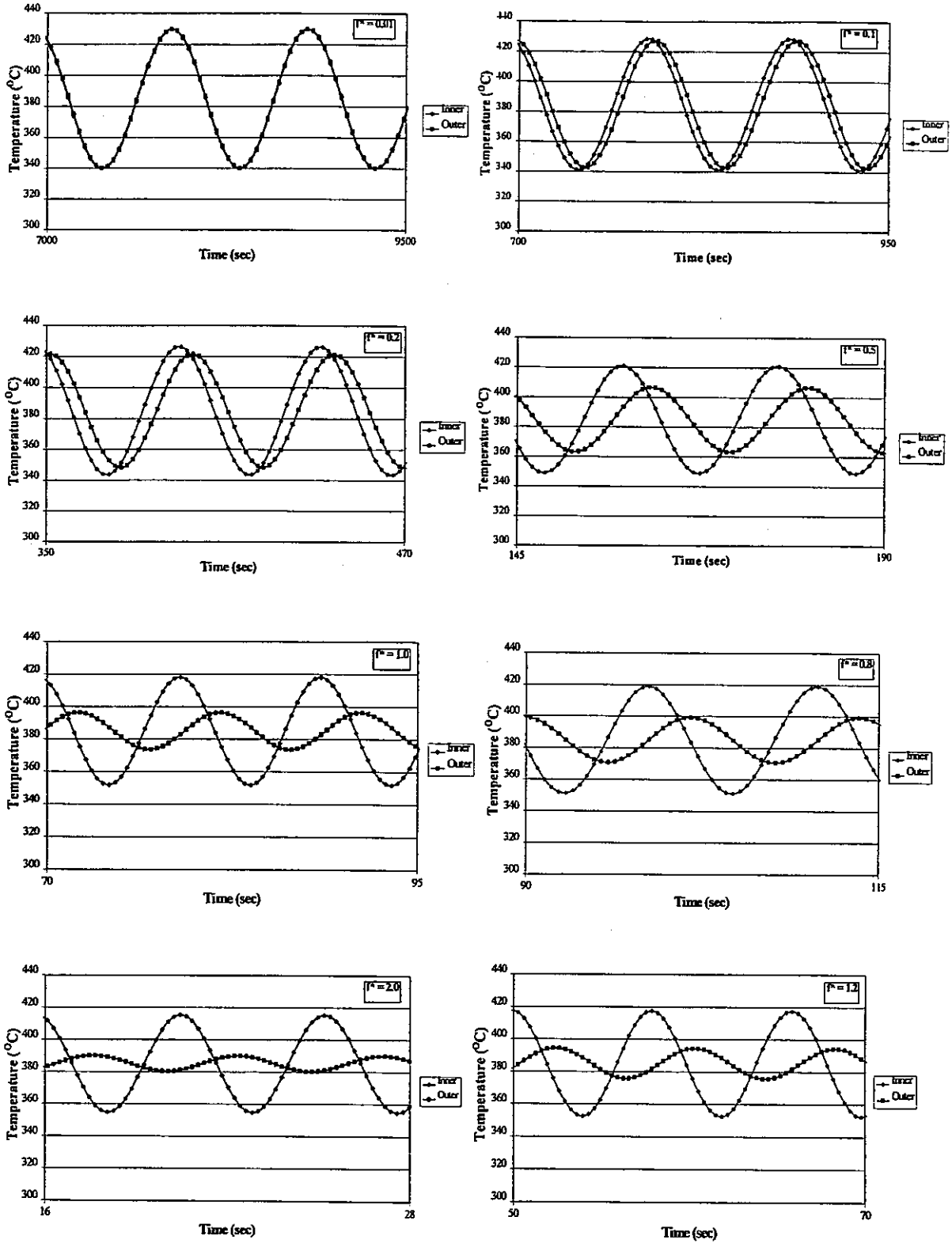

Fig.20 History of Temperature of Non-dimensional frequency f* = 0.01, 0.1, 0.2, 0.5, 0.8, 1.0, 1.2 and 2.0 when Biot number = 6.0 (FEM)

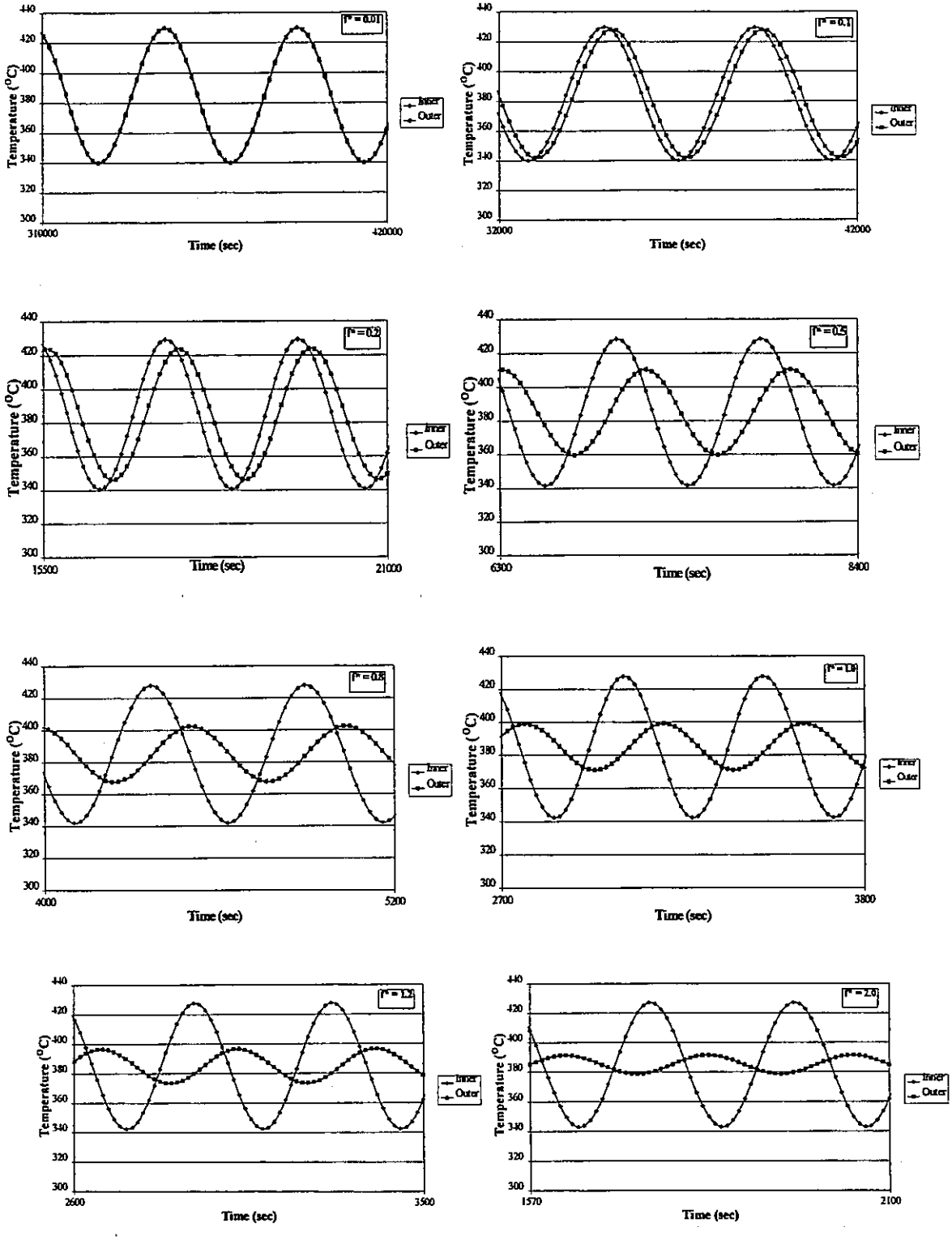

Fig.21 History of Temperature of Non-dimensional frequency f* = 0.01, 0.1, 0.2, 0.5, 0.8, 1.0, 1.2, and 2.0 when Biot number = 40 (FEM)

6. Conclusions

Frequency response characteristics of structures and its mechanism were investigated by both numerical and theoretical methods. Based on above investigation, a structural response diagram was derived, which can predict stress amplitude of structures from temperature amplitude and frequency of fluids. Furthermore, this diagram was generalized to be the Non-dimensional structural response diagram (NSRD), by introducing non-dimensional parameters such as Biot number (Bi) , non-dimensional frequency (f*), and non-dimensional stress (σ *). Accuracy of NSRD was verified through comparison with F.F. calculated results.

The use of the NSRD appears to evaluate thermal stress caused by thermal striping, rapidly without structural analysis, and rationally with considering attenuation by non-stationary heat transfer and thermal unloading. Additionally, the NSRD can give useful information as sensitive frequency range to adjust coupled thermohydraulic and thermomechanical analysis models for consideration of such attenuation factors as turbulent mixing, molecular diffusion, non-stationary heat transfer, and thermal unloading.

Acknowledgement

The authors wishes to express his gratitude to Mr. Ichiro Furuhashi of CRC Research Institute Inc. for several helpful discussions in the field of theoretical analysis. Thanks are due to participants of the IAEA coordinated research program on "Harmonization and Validation of Fast Reactor Thermomechanical and Thermohydraulic Codes and Relations Using Experimental Data", with whom we have discussed this problem.

References

[1] Muramatsu,T., 'Evaluation of Thermal Striping Phenomena at a Tee Junction of LMFR Piping System with Numerical Methods (1) Thermohydraulic Calculations, SmiRT15, Div.F (to be published)

[2] Kasahara,N., 'Evaluation of Thermal Striping Phenomena at a Tee Junction of LMFR Piping System with Numerical Methods (2) Thermomechanical Calculations ', , SmiRT15, Div.F (to be published)

[3] Iwata, K. and Tsukimori, K, 'FINAS Version 12.0 User's Manual', PNC TN9520 95-013, (1995)

[4] Lejeail, Y., et al., 'A contribution to improvement of design rules on thermal striping', SMiRT14, Lyon,(1997)

[5] Boley, B.A., 'Theory of Thermal Stresses', John Wiley & Sons,(1960)

[6] Holman, J.P, "Heat Transfer", 7th ed., McGraw-Hill, (1990)

[7] Norimatsu.,S., et.al.,'High-cycle non-steady thermal stress analysis – Thermal transient test on sodium components (XI)', PNC ZN941 77-57, In Japanese, (1997)